

## Bifurcation phenomena in nonaxisymmetric Taylor-Couette flow

Philip W. Hammer,\* Richard J. Wiener,† and Russell J. Donnelly

Department of Physics, University of Oregon, Eugene, Oregon 97403

(Received 9 July 1992)

Taylor-Couette flow subject to a nonaxisymmetric external Coriolis force is studied experimentally. The Coriolis force is induced by placing the Taylor-Couette apparatus on a turntable such that the flow is nonaxisymmetrically perturbed. This symmetry-breaking perturbation affects the entire sequence of bifurcations found in the unperturbed system. We identify the dynamical regimes encountered as a function of two control parameters: a Reynolds number and a dimensionless turntable rotation rate. The bifurcation map for this system is presented, and we show that there is nonhysteretic reemergent order as a function of either control parameter. We also find a possible codimension-2 bifurcation point beyond which occurs a nonhysteretic direct bifurcation to turbulence from the time-independent base flow.

PACS number(s): 47.20.Tg, 47.25.Ae, 47.30.+s

### I. INTRODUCTION

Externally applied potential fields are known to have profound effects on the stability of hydrodynamic systems. Flows that have received considerable attention, both experimentally and theoretically, include Rayleigh-Bénard convection (the flow between horizontal parallel plates, heated from below) and Taylor-Couette flow (the flow in the annular gap between independently rotating concentric cylinders) [1]. Both the Rayleigh-Bénard (RB) and Taylor-Couette (TC) systems have been subject to an external magnetic field. It was found that the base state is stabilized, and the ordinary bifurcation behavior seen in the unperturbed system is significantly altered [2,3]. In the case of an applied magnetic field  $\mathbf{H}$  (where the Lorentz force  $\mathbf{F}_L \sim \mathbf{H} \times \mathbf{u}$  acts), the working fluid is conducting—mercury, for example. The RB system has also been placed in a rotational field,  $\Omega_D$  (where the Coriolis force  $\mathbf{F}_C \sim \Omega_D \times \mathbf{u}$  acts). Again, the base state is stabilized, and other interesting bifurcation phenomena have been encountered as well [4,5].

Chandrasekhar made important early contributions to this field of study [1]. By unifying theory and experiments from a wide variety of flows and applied external fields, he set the stage for much of the research carried out subsequently. The research of Chandrasekhar and his colleagues on linear stability has evolved and expanded to contemporary studies of spatiotemporal chaos, turbulence, pattern formation, and bifurcations. Such studies have had important implications to open and closed flows as well as to magnetohydrodynamics and plasmas. Understanding the effects of symmetry breaking and mode competition has also become important.

By applying a *nonaxisymmetric* external Coriolis force to the Taylor-Couette system, we have initiated an important extension to the study of external perturbations on hydrodynamic flows [6]. The Coriolis force is applied to the TC system by placing the cylinders on a turntable so that the cylinders' common axis of rotation is orthogonal to the rotational axis of the turntable (see Fig. 1). In

the Appendix we discuss the reasoning behind this orientation of the cylinders relative to the turntable. In *ordinary* TC flow (defined to be TC flow with only the inner cylinder rotating and no applied field), the fluid velocity in the base state is purely azimuthal because the flow direction is determined by the direction of the inner-cylinder rotation and the boundary conditions [7]. This azimuthal base flow is called "Couette flow." When the system is placed on a rotating turntable, the ordinary velocity field interacts with the rotational field, yielding a Coriolis force. To first order in  $\Omega$  (where  $\Omega$ , to be defined below, is a dimensionless measure of the Coriolis force), the Coriolis force is axial, and it induces a corresponding axial flow superimposed on the Couette flow [8]. The Coriolis force is not unidirectional, however; as the fluid flows about the azimuth, it changes direction with respect to the turntable rotation vector. The axial component of the modified base state changes direction correspondingly, both in magnitude and direction, with the azimuthal angle. The axisymmetry of the ordinary TC system is thereby broken.

As the Reynolds number (a dimensionless measure of the inner-cylinder speed) is slowly increased from zero,

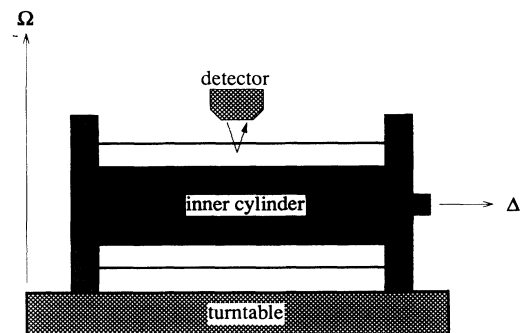


FIG. 1. Side-view schematic of the experimental configuration, showing the orientation of the cylinders relative to the turntable and the orientation of the reflectance detector.

the *ordinary* TC system displays a series of bifurcations that lead to increasingly complex spatiotemporal behavior and eventually turbulence [9]. Our experiments prior to those reported here have shown that the introduction of a small Coriolis force dramatically alters this sequence of bifurcations. The Coriolis force stabilizes both the base flow [6] and the bifurcation to the first time-dependent state [8]. In addition, the stability of the base state in the presence of a Coriolis force has been predicted theoretically [10,11]. In this article we report that at low values of either control parameter (the Reynolds number or  $\Omega$ ), the flow displays reemergent order from temporally disordered flow. We have also observed a possible codimension-2 bifurcation point beyond which there occurs a direct, nonhysteretic bifurcation to turbulence from the base flow state [8]. Codimension- $m$  bifurcations are found in  $m$ -control parameter systems and are characterized by mode competition resulting from multiple modes becoming simultaneously unstable [12,13]. For a sufficient value of  $\Omega$ , the direct bifurcation to turbulence occurs at a Reynolds number that is an order of magnitude lower than that for ordinary TC flow. These phenomena also occur at a relatively small values of the control parameters, so that they might be understood via numerical simulation or a weakly nonlinear theory.

In this article we will report of our studies, building on work by our group [6,8,10] and that of Ning and his colleagues, who have carried out similar studies in different geometries [11,14,15]. Section II places our experiments in the context of ordinary TC flow and then follows with a review of the previous work on nonaxisymmetric TC flow that led up to our research. In Sec. III we present the relevant experimental parameters and the experimental protocol we implemented. In Sec. IV we describe the statistics and analysis we used to derive a picture of the flow bifurcation behavior. In Sec. V we discuss the important features of the bifurcation map, in particular, our discovery of reemergent order and the direct bifurcation to turbulence. Concluding remarks are made in Sec. VI. In the Appendix we present theoretical and experimental results for the configuration in which the cylinder and turntable axes are parallel. This appendix clarifies the importance of the cylinder-turntable positioning we have employed to study nonaxisymmetric TC flow.

## II. BACKGROUND AND PREVIOUS WORK

### A. Bifurcations in ordinary Taylor-Couette flow

Ordinary TC flow displays a series of bifurcations that progress toward turbulence from Couette flow as the inner-cylinder angular velocity is slowly increased from zero. Couette flow exists for Reynolds numbers  $Re$  less than the critical Reynolds numbers  $Re_{c0}$  and is purely azimuthal; the flow displays no spatial or temporal periodicity. At  $Re=Re_{c0}$ , the base state becomes centrifugally unstable and the flow bifurcates to Taylor vortex flow (TVF), which consists of axially periodic, time-independent toroidal vortices superimposed on the azimuthal flow. Note that  $Re_{c0}$  is a function of the inner-

to outer-cylinder radius ratio,  $\eta$ . In our work,  $\eta=0.88$  and  $Re_{c0}=120.5$  [9,10]. At about  $Re=1.14Re_{c0}$ , there is a Hopf bifurcation which results in a traveling azimuthal wave superimposed on the Taylor vortices. This state, wavy vortex flow (WVF), persists until about  $Re=10Re_{c0}$ .

The WVF eigenstate can be expressed in terms of an azimuthal wave number, which describes the number of waves wrapped around the azimuth, and an axial wave number, which is proportional to the number of wavy vortices stacked up in the annulus. King and Swinney have shown that the eigenstate of a particular wavy mode is dependent on both the Reynolds number and the number of vortices [16]. They also found that there are regions in this state space where the wavy vortices are unstable. King and Swinney's findings were consistent with those of Donnelly *et al.*, who found disordered states that emerged hysteretically in the wavy mode for small bands of Reynolds numbers [17]. They observed a dislocation in the flow which mediated transitions in the wavy mode from one state to another. These transition regions were also characterized by broadband noise in the velocity power spectra.

At  $Re\cong 10Re_{c0}$ , WVF bifurcates to modulated wavy vortex flow (MWVF) in which a second azimuthal wave appears in the flow whose frequency is incommensurate with the first [18]. This quasiperiodic state appears visually as an amplitude modulation of the primary wave. It is this beat frequency which is seen in the power spectra. The pure modulated state persists until about  $Re\cong 12Re_{c0}$ , at which a broadband component emerges in the velocity power spectrum, accompanied by an elevation in the spectral noise level above the instrumental noise level [19]. It has been shown that this spectral noise is deterministic, as opposed to stochastic [20]. This finding and the broadband character of the power spectrum, coupled with further analysis of the time series, have led to the conclusion that this state is dynamically low dimensional, i.e., chaotic [20].

At  $Re\cong 21Re_{c0}$  all spectral evidence of periodicity in the flow disappears and the flow is characterized as turbulent [20]. Note, however, that the axial array of Taylor vortices does not disappear in this turbulent state. In fact, Taylor vortices have been observed beyond  $Re=67Re_{c0}$  [21]. In addition, Walden and Donnelly found that for Reynolds numbers approximately between  $28Re_{c0}$  and  $35Re_{c0}$ , a distinct periodic component reemerges in the power spectrum [21].

### B. Previous studies of nonaxisymmetric Taylor-Couette flow

Bifurcations in ordinary TC flow have been well researched ([9,16–21], and references therein). As mentioned in the Introduction, several studies have been undertaken to examine variations on the TC theme, most of which have been axisymmetric. Mutabazi *et al.* have studied the stability and bifurcation behavior of the Taylor-Dean system (flow between horizontal coaxial

cylinders with a partially filled gap) which is nonaxisymmetric [22]. The base state in the Taylor-Dean system can be thought of as a superposition of Taylor-Couette flow and Poiseuille flow. The bifurcation phenomena observed in the Taylor-Dean system have been attributed to mode competition resulting from the combined flows [22]. However, the Taylor-Dean system, while displaying a distinct nonaxisymmetry, cannot be treated as perturbation of the ordinary TC system because the base state is significantly altered by the partially filled gap. Our research was initiated by an interest in the effect of a nonaxisymmetric perturbation (whose strength is tunable by a control parameter and varies continuously from zero) on the stability of the base state of the ordinary TC system and on the subsequent bifurcation behavior.

The experiments of Wiener *et al.* (performed at  $\eta=0.88$ ) showed that for small  $\Omega$  (i.e.,  $\Omega < 2.5$ ), the base flow is stabilized quadratically in  $\Omega$  [6]. For  $2.5 < \Omega < 7$ , higher-order effects cause the stabilization to become stronger than quadratic, and then for  $\Omega$  above 7, the stability boundary has an inflection point and then becomes weaker than quadratic. Beyond this primary bifurcation boundary and within the range of  $\Omega$  that yields time-independent secondary flow, the system bifurcates to *tilted* Taylor vortices (TTVF). This state is similar to TVF except that the Coriolis force induced axial perturbation imposes a tilt on the Taylor vortices such that the vortices are tilted out of the cylinders' axial plane. Ning *et al.* showed that at  $\eta=0.753$  and at constant  $Re$ , the tilt angle of the vortices increases linearly with  $\Omega$  [15]. We observed increasing tilt angle with  $\Omega$  at  $\eta=0.88$ , but did not make any quantitative measurements of this effect. Note also that we imposed hard boundary conditions at the ends of the cylinders, thus requiring the tilt angle to be zero at the boundary. We thus observe a maximum tilt at the center of the cylinders and a tilt angle that decreases as the ends are approached.

In addition, Wiener *et al.* obtained preliminary results showing that the bifurcation to time-dependent flow is also delayed as the strength of the Coriolis force increased [8]. For  $\Omega > 0$ , the first periodically time-dependent state encountered is *tilted* wavy vortex flow (TWVF). Again, this state is a single-frequency flow similar to WVF, except here the wavy vortices are tilted due to interactions with the axial flow. In addition, we found that the primary stability boundary and the boundary for the bifurcation to time-dependent flow converged as  $\Omega$  increased [8]. Beyond this convergence, the flow bifurcated directly to turbulence from the time-independent base state [8].

These initial experiments were followed by theoretical studies aimed at understanding the effect of the Coriolis force on Couette flow [8]. This was followed by a linear stability analysis on the resulting modified base flow [10,11]. Wiener *et al.* found that to first order the Coriolis force induces an axial flow which is superposed on the azimuthal Couette flow. The magnitude of the axial flow varies as an  $m=1$  sinusoid about the azimuth [8]. This first-order correction to the base state is orthogonal to the azimuthal mode, and it is the interaction and competition between these orthogonal modes which gives rise

to much of the dynamics we observed in nonaxisymmetric TC flow.

To investigate theoretically the stability of the modified base flow, Wiener *et al.* perturbed the solution with small  $\Omega$ -dependent velocity and pressure fields. The perturbations were three dimensional and time dependent. The perturbed base flow was expanded to order  $\Omega^2$ , and a linear eigenvalue problem was constructed for the stability problem. The problem was separable into zeroth-, first-, and second-order terms. The zeroth-order term returned  $Re_{c0}$ . The first-order correction to the critical Reynolds number was found to be zero, which is consistent with the symmetry of the perturbation, i.e., the effect of the Coriolis force is not dependent on the direction of the turntable rotation. The second-order correction was the first surviving higher-order term, such that for small  $\Omega$ ,  $\Delta = c_R \Omega^2$ , where  $c_R = 0.04363$  and  $\Delta = (Re_c / Re_{c0}) - 1$ . This theoretical result is in good agreement with experimental results for small values of  $\Omega$  [10]. Ning *et al.* conducted parallel studies and obtained compatible results [11]. The linear stability analysis has been taken to order  $(\Omega^4)$  by Tveitereid, Ning, and Ahlers, and their theory is also in good agreement with experimental results [23]. In Fig. 2 we have compared our experimental measurements of the primary bifurcation (boxes) to the theoretical prediction of Wiener, Hammer, and Tagg (solid curve) [10], and to the prediction of Tveitereid, Ning, and Ahlers (dashed curve) [23]. From the figure it can be seen that the theory of Wiener, Hammer, and Tagg agrees with the experimental data for  $\Omega \lesssim 2.25$ . The theory of Tveitereid, Ning, and Ahlers is in agreement with experiments for  $\Omega \lesssim 3.5$ .

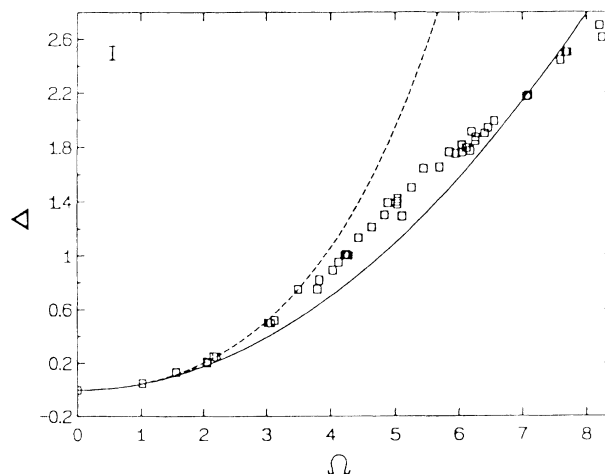


FIG. 2. Comparison of experiment and theory for the primary instability at  $\eta=0.880$ . The squares are the experimental data. The solid curve is the second-order theoretical stability boundary of Wiener, Hammer, and Tagg [10], and the dashed curve is the fourth-order calculation of Tveitereid, Ning, and Ahlers [23]. For the solid curve,  $\Delta=0.04363\Omega^2$ ; for the dashed curve,  $\Delta=0.04551\Omega^2+0.001281\Omega^4$ . The error bar represents an estimate of the experimental uncertainty.

### III. EXPERIMENTAL PARAMETERS AND PROTOCOL

#### A. Definition of the control parameters

Figure 1 represents the apparatus used in the experiments reported here. The fluid used in our experiments was an aqueous suspension of glycerol and Kalliroscope, with bacteriostatic stabilizer added to extend the life of the sample [24]. Kalliroscope is a suspension of highly reflective, microscopic platelets and is used for flow visualization experiments. Typically, the working fluid had kinematic viscosity  $\nu=0.033$  S. The inner-cylinder angular velocity was scaled by a reduced Reynolds number  $\Delta=(\text{Re}/\text{Re}_{c_0})-1$ , where  $\text{Re}=\omega R_1 d/\nu$  ( $\omega$  is the inner-cylinder angular velocity,  $R_1=2.235$ , cm is the inner-cylinder radius, and  $d=0.305$  cm is the annular gap width).  $\text{Re}_{c_0}$  is the critical Reynolds number at which the primary instability from the base flow to Taylor vortex flow occurs in ordinary TC flow. Recall that  $\text{Re}_{c_0}=120.5$  for the radius ratio  $\eta$  we used ( $\eta=0.88$ ) [9,10]. Another important parameter is the aspect ratio of the apparatus,  $\Gamma$ , which is the ratio of the length of the annulus to  $d$ . The angular velocity of the turntable is scaled by  $\Omega=\Omega_D d^2/\nu$  (where  $\Omega_D$  is the angular velocity of the turntable).  $\Omega$  can also be thought of as a dimensionless measure of the amplitude of the Coriolis force for a given Reynolds number.

#### B. Temperature control

In order to minimize temperature-induced fluctuations in the viscosity, and hence uncertainty in the critical Reynolds number, we housed the cylinders in an insulated box and maintained the brass end caps of the apparatus at constant temperature with a circulating temperature bath. The inner-cylinder motor was kept external to the insulated box to further isolate the fluid from sources of heat. These precautions resulted in temperature stability during a data run to within  $\pm 0.1$  K. The temperature of the fluid during the entire series of experiments ranged from 23.4 to 24.2°C. Within this range of temperatures, our uncertainty in  $\nu$  was about 0.6%, which translates to a comparable uncertainty in  $\text{Re}_{c_0}$ . Our apparatus also had an axial temperature gradient. With the cooling of the end caps, we were able to keep the gradient to less than 0.2 K. Other factors, the details of which can be found in Ref. [25], contributed to an uncertainty in  $\omega_{c_0}$  of about 0.8%. Finally, note that Ref. [25] also contains a more detailed description of the experimental apparatus and procedures.

#### C. Protocol: Quasistatic Increments of $\Omega$ and $\Delta$

In our experiments we quasistatically increased one of the parameters ( $\Omega$  or  $\Delta$ ) at small increments, while holding the other parameter fixed. At each increment of  $\Omega$  or  $\Delta$ , a 2048-point time series of the Kalliroscope reflectance was measured (increased occasionally to 8192 points). The data acquisition frequency was  $50(\omega/2\pi)$ . From the time series we were able to calculate the various statistical measures that we used to determine the location of the bifurcation boundaries for this system.

It is important here to clarify what we mean by “quasistatic increments” in our experimental control parameters. Fluid dynamic states require a finite time in which to fully develop, that is, a change in  $\text{Re}$  causes a change in  $\mathbf{u}$  which takes time to propagate, even in the base state. Thus the time rate of change of a control parameter must be much smaller than the growth rate of a particular state. Also the bifurcations to TVF and WVF are nonhysteretic in the Reynolds number, *if*  $\text{Re}$  is increased slowly enough, i.e., quasistatically. Therefore, a criterion was needed to minimize the hysteresis in the flow bifurcations.

The effect of the Reynolds number rate of change,  $a^*$ , on the bifurcation to TVF was studied by Park, Crawford, and Donnelly [26]. They defined  $a^*$  to be

$$a^* = \frac{R_1 d^3 \Gamma}{\nu^2} \langle \alpha \rangle, \quad (1)$$

where  $\langle \alpha \rangle$  is the average time rate of change of  $\omega$ . Their experiments showed that if  $a^*$  is too large (i.e., if the Reynolds number is increased through the bifurcation to TVF too rapidly), then the critical Reynolds number will be overestimated. Similarly, if  $\text{Re}$  is decreased from TVF to the base flow state too rapidly, then  $\text{Re}_{c_0}$  will be underestimated. The difference between these two critical Reynolds numbers is proportional to the hysteresis for that  $a^*$ . Park, Crawford, and Donnelly found an upper limit on  $a^*$  at which the critical Reynolds numbers for increasing and decreasing  $\text{Re}$  agreed to within an acceptable percentage. Their conclusion was that  $a^* < 6$  is sufficient to minimize the hysteresis in the first bifurcation [26].

In subsequent work, Park and Jeong showed that  $a^* < 1$  is needed to get repeatable and nonhysteretic results for the bifurcation to WVF [27]. By repeatable, they meant that different experiments would yield states with the same axial and azimuthal wave numbers, that is,  $a^* < 1$  resulted in reproducible eigenstates of the system.

In the Coriolis-force experiments reported here and elsewhere [6,8,10], the above criteria for quasistatic increases in  $\text{Re}$  were used, except that repeatability in the wavy-mode eigenstate was not required. This requirement was dropped because our experiments were designed to locate bifurcations; as such, the dynamics of the various states were not examined closely.

In initial experiments on the primary bifurcation (base flow to secondary flow), Wiener *et al.* obtained results that showed that  $a^* \leq 6$  yielded nonhysteretic bifurcations [6]. In the experiments reported here we chose  $a^* \cong 0.66$  so that we could confidently attain nonhysteretic bifurcations to and from time-dependent states as well.

Wiener *et al.* also found that the bifurcations were insensitive to the acceleration of the turntable,  $\delta\Omega/\delta t$  [6,8,10]. However, in Sec. V A we report that we did observe slight  $\Omega$ -dependent hysteresis across one of the bifurcation boundaries. Also, Ning, Ahlers, and Cannell observed  $\Omega$ -dependent hysteresis in the transition to what they refer to as “chaotic tilted vortices” [14]. Note, however, that their experiments were performed on an apparatus with  $\eta=0.753$  and with different boundary conditions. Thus, the chaotic tilted vortices they reported

could have resulted from the dynamics of this larger gap system. For our experiments we chose  $\delta\Omega/\delta t = 0.00196 \text{ s}^{-1}$ , and we generally did not observe any significant  $\Omega$ -dependent hysteresis.

#### IV. ESTABLISHING THE BIFURCATION MAP

##### A. Locating bifurcations using reflectance

Our goal in the series of experiments reported here was to establish a bifurcation map for the nonaxisymmetric TC system. Previous work had shown that the Coriolis force perturbs the system in profound ways [6,8,10,11,14,15], and analogies to other work, such as that on the Küppers-Lortz transition in rotating RB convection [5], suggest that an exploration of parameter space would reveal unexpected bifurcations to novel spatiotemporal states.

As mentioned in Sec. III, our analysis is based on measurements of Kalliroscope reflectance. In water-glycerol mixtures, Kalliroscope is a suspension of nearly neutrally buoyant microscopic platelets [24]. The platelets align with the shear in a flow and give the fluid a highly reflective pearlescent sheen. When the ordinary TC system is in its azimuthal base state, the flow is laminar and the platelets are aligned such that the normal to their broad plane is, on average, aligned radially. In this orientation of the platelets, an external light-intensity detector aligned tangential to the glass outer cylinder and normal to both the cylinder radius and cylinder axis will measure relatively high reflectance. In Couette flow, one thus observes a uniform silvery flow, which is consistent with the absence of spatial or temporal structure to the flow. When the bifurcation to TVF or TTVF occurs, there is an onset of radial inflow and outflow jets that results in the toroidal vortices. The Kalliroscope platelets partially realign with this radial flow and one observes silvery tori separated by darker bands corresponding to the alternating inflow and outflow boundaries (see Ref. [9], p. 140, and Ref. [13] for photographs of states from ordinary TC flow). Measurements reveal that at the bifurcations to TVF and TTVF, there is a sharp drop in the average reflectance,  $\langle r \rangle$ , due to this realignment of the platelets.

When the flow is in a time-independent state, the fluctuations of the reflectance about the average are relatively small. The platelets do have some random wobble, but our detector measures an area that is large compared to both the size of a platelet and the amplitude of the wobbles. This measurement technique has the effect of spatially averaging the small-scale random wobbles of the platelets. At the onset to a time-dependent state the fluctuations about the average of the reflectance increase measurably and significantly. Accordingly, there is a sharp increase in the variance of the reflectance,  $\sigma^2$ , at the bifurcation to time dependence, relative to that measured in a time-independent state.

By making systematic comparisons of relative changes

in the average reflectance and the variance of the reflectance, we can accurately determine the parameter values for the primary bifurcation and the bifurcation to time dependence, respectively. Within the time-dependent flow state, however, there are both periodic and aperiodic states. We thus required additional information to distinguish among these various states.

Gorman and Swinney have shown that a fast Fourier transform (FFT) of a reflectance time series from a periodic or quasiperiodic state in ordinary TC flow will reveal accurate frequency information about the flow [18]. While it is unclear whether Kalliroscope reflectance will yield accurate information about the dynamics of a disordered flow, the work of Savas [28] and of Schwarz [29] do show that the motion of Kalliroscope flakes is connected to the underlying structure of both ordered and turbulent flows. Based on the above studies and findings we will discuss below, we have adopted the view that *relative* changes in well chosen statistics will indicate bifurcations to different flow regimes. The average and the variance of the reflectance are two such statistics. To locate bifurcations between periodic (ordered) states and aperiodic (disordered) states, additional statistics are required.

The character of a time-dependent state is most immediately seen by examining its reflectance power spectrum. A power spectrum of the base flow and TTVF in the nonaxisymmetric TC system (both time independent) is characterized by instrumental noise and peaks indicating the frequency of the inner cylinder. The appearance of the inner-cylinder frequency is an experimental artifact: The inner cylinder is composed of black anodized aluminum; when the cylinder was first constructed, it was uniformly black, but within a short time the blackness lost its uniformity and the inner cylinder was no longer optically round. We attribute this loss of optical uniformity to a thin layer of Kalliroscope platelets adhering to the cylinder in places where there were small divots in the anodization. Fortunately, we could essentially ignore the presence of the inner-cylinder frequency in these power spectra, since our goal was to identify relative changes in power spectra for a large range in control parameters. The presence of the inner-cylinder frequency in the power spectra does not affect these measurements.

Power spectra for TWVF are characterized by sharp peaks representing the wave frequency and its harmonics. Also present are sum and difference peaks for the wave and inner-cylinder frequencies. The noise in these power spectra is still at the instrumental level. Power spectra from TWVF can be contrasted to those from aperiodic or disordered states which are characterized by significant increases in the noise level. In nonaxisymmetric TC flow the strength and distribution of the noise level vary continuously as the spatiotemporal disorder increases towards turbulence, but in all cases the noise level is higher than the instrumental noise. To measure relative changes in the spectral noise and the power distribution among the spectral components, we used two statistics: the spectral mode number (SMN) and the spectral number distribution (SND).

The SMN is given by

$$D = \frac{\left( \sum_{i=1}^n P_i \right)^2}{\sum_{i=1}^n P_i^2}, \quad (2)$$

where  $P_i$  is the amplitude of the  $i$ th Fourier component of an  $n$ -component power spectrum. The SMN is a slight variation on the “degrees of freedom” used by several authors as a tool to detect changes in the disorder in a flow. Crutchfield *et al.* used the degrees of freedom in an attempt to distinguish sharp features from broad features among power spectra from the Rössler system (the Rössler system will be described below) [30]. Their results were inconclusive, but Park and Donnelly successfully used a similar measure to detect the bifurcation from laminar flow to TVF [31]. Park and Donnelly were concerned with relative changes in the degrees of freedom as a signature of bifurcation, whereas Crutchfield *et al.* only hinted at this application. Babcock, Ahlers, and Cannell used a statistic similar to the SMN to locate the boundary separating the convective and absolute instabilities in TC flow with a superimposed axial through flow [32]. Note also that the measurements of Park and Donnelly, and of Babcock, Ahlers, and Cannell were based on Kalliroscope reflectance.

We have carried out a study of the SMN and found that it provides a rough measure of the number of dominant peaks in a power spectrum. Ideally,  $D=1$  for a sine wave and  $D=n$  for white noise. Our study consisted of calculating  $D$  as a function of the number of sine waves in a given numerical signal, with and without the addition of varying amounts of noise. The signals we analyzed were composed of 1 to 99 sine waves linearly superimposed with frequencies ranging from 5 to 490 Hz at 5-Hz intervals. Each time series consisted of 4096 points. The power spectra had 512 points resulting from four averaged of 1024-point FFT's. The Nyquist frequency was 500 Hz. For the case of an increasing number of sine waves without the addition of noise, we found that  $D$  is roughly equal to two times the number of sine waves in the signal.

After looking at the effect of summing pure sine waves, we looked at the effect on the SMN of noise added to the summed waves. We summed the specified number of sine waves and then added random noise with a normal distribution to this signal. This numerical experiment was performed at four different noise levels: 0.5, 1.0, 2.0, and 3.0 times the amplitude of the combined sine waves. Figure 3 shows the SMN as a function of the number of combined waves plus the added noise. The result for a noiseless signal is also shown for comparison. The clean signal shows a linear increase in the SMN as the number of waves increases. Adding 0.5 amplitude noise had the effect of shifting the SMN slightly up and changing the slope of the line such that the influence of noise was greatest for smaller numbers of combined waves. As the amplitude of the noise was increased, its effect on the SMN became more pronounced. This was especially true for smaller numbers of combined signals, where the noise dominated the periodic component of the signal, causing

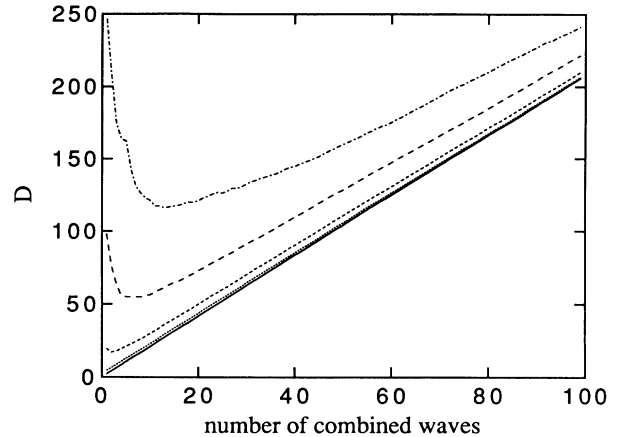


FIG. 3. The spectral mode number  $D$  (where  $D$  is dimensionless) plotted as a function of the number of combined waves. The solid curve is for combined sine waves with no added noise. The dotted curve is for sine waves combined with half-amplitude random noise. The short-dashed curve is for random noise of equal amplitude added to the combined sine waves. The long-dashed curve and the dot-dash curve are for random noise of amplitude two and three times that of the combined sine waves, respectively.

the SMN to be large. As the number of waves was increased, the SMN rapidly decreased until it reached a minimum. Beyond this minimum, the SMN then gradually increased with a slope approximately equal to that of the clean signal, only shifted by a constant value dependent on the strength of the noise. Clearly then, the SMN is a useful statistic for distinguishing among periodic signals of increasing complexity and noise.

To complement the SMN, we chose the SND as another statistic that might provide us with similar information about relative changes in the degree of order or disorder in the flow. The SND was developed as a variation of the spectral distribution function used by Ditto *et al.* [33]. The SND is found by counting the number of components  $N(p)$  in a power spectrum that have power greater than or equal to  $p$ , where  $p = \log_{10}(P)$ , and  $P$  is the Fourier amplitude. The SND is useful for examining changes in the distribution of spectral components as a system evolves from one composed of a single mode to one composed of multiple modes. The SND is useful for looking at the distribution of spectral components as deterministic noise begins to dominate a power spectrum.

The differences in the SND profile are most striking when comparing the profile for a sine wave to that for random noise (see Fig. 4). For a single-mode sine wave, all of the energy in the spectrum should be found in one sharp, narrow peak (ideally a delta function). This highly localized distribution of power in the spectrum should be evident as a decrease in the SND as the power increases [see Fig. 4(a)]. This dropoff is indicative of a nonuniform distribution of power with respect to frequency. The slope of the dropoff is related to the narrowness of the peak, i.e., the steeper the slope, the narrower the spectral peak. The SND profile for random noise, on the other

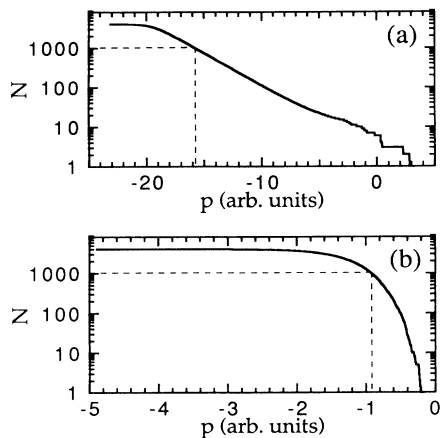


FIG. 4. Spectral number distributions for (a) a sine wave and (b) random noise. The horizontal dashed lines indicate  $N=0.25n$ , where  $n=4096$ . The vertical dashed lines indicate the spectral noise (see text, particularly that pertaining to Fig. 6): (a) spectral noise =  $-15.75$ , and (b) spectral noise =  $-0.91$ .

hand, stays level, then drops off sharply, indicating that the power in the spectrum is more evenly distributed throughout its range [Fig. 4(b)]. The power at which  $\log_{10}(N(p)) \cong 0$  is the saturation power. Figure 4 indicates that a periodic system saturates gradually, while a noisy system will saturate quickly beyond a certain power.

Besides being useful for comparing the power distribution of different spectra, the SND can be used as a means of estimating the relative spectral noise level among spectra. To measure the spectral noise, we adopted the following criterion: After calculating the SND, we choose the spectral noise to be the power  $p$  at which  $N(p)$  drops below  $0.25n$ , where  $n$  is the number of components in the power spectrum (see Fig. 4 for an example). In other words, a criterion of  $0.25n$  means that 25% of the spectral components have power less than a given power  $p$ . Our choice of  $0.25n$  as the cutoff for the spectral noise measurement was made as an attempt to systematize the noise estimate that one typically makes "by eye" when examining power spectra. As we shall explain, the 25% criterion provided a useful means for detecting relative changes in the spectral noise.

The 25% criterion for measuring the spectral noise provided us with a systematic and efficient means for measuring the relative degree of disorder among many points in  $\Omega$ - $\Delta$  space. The spectral noise measurement was also robust with respect to where we chose the cutoff. That is, we were able to obtain consistent results in a variety of systems for  $0.10 < x < 0.80$ , where  $x$  determines the percentage of  $n$  at which the cutoff is made. So although our choice of  $0.25n$  was arbitrary, it did reliably yield the information we desired about the relative disorder among different dynamical states of the same system.

In an attempt to study a system more complex than the combined sine waves, and one that was nonlinear, we chose the Rössler system. The Rössler system is de-

scribed by three coupled nonlinear ordinary differential equations,

$$\begin{aligned} \frac{dx}{dt} &= -(y+z), \\ \frac{dy}{dt} &= x+0.2y, \\ \frac{dz}{dt} &= 0.2+xz-\mu z. \end{aligned} \quad (3)$$

As the control parameter  $\mu$  is varied, the system undergoes a series of period-doubling bifurcations. Throughout the periodic regimes the largest nonzero Lyapunov exponent is negative (i.e., the system is non-chaotic). At a critical value of  $\mu$  the largest Lyapunov exponent becomes positive and the system bifurcates to chaos. Figure 5, which was motivated by Fig. 1 of Ref. [30], shows the power spectra and  $x$ - $y$  phase portraits of the four Rössler states we analyzed. Figure 5(a) is a period-2 state, Fig. 5(b) is a period-4 state, Fig. 5(c) shows chaotic broadening of the period-4 state, and Fig. 5(d) shows chaotic broadening of the period-2 system. The Rössler system is useful as a more complicated system with which we could check both the SMN and the SND. For example, we examined various dynamical states of the Rössler system as a means to test the robustness of our spectral noise measurement technique.

To test the robustness of the spectral noise measurement, we calculated the spectral noise as a function of cutoff percentage for the four different states of the Rössler system we examined (see Fig. 6). The solid curve corresponds to Fig. 5(a), the dashed curve to Fig. 5(b), the dotted curve to Fig. 5(c), and finally, the dot-dash curve corresponds to Fig. 5(d). The curves are presented in order of increasing complexity. Figure 6 conveys that the spectral noise does increase as the Rössler system becomes more chaotic. The other important aspect of Fig.

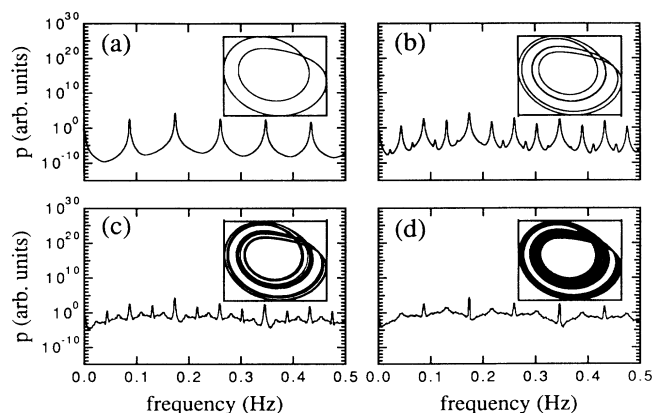


FIG. 5. Four states of the Rössler system as a function of the adjustable parameter  $\mu$  and initial conditions  $(x_i, y_i, z_i)$ . Shown are the power spectra, with the  $x$ - $y$  phase portraits inset, for (a)  $\mu=3.5$  (3.3425, 2.9585, 1.2043); (b)  $\mu=4.1$  (4.0902, 2.1835, 0.5043); (c)  $\mu=4.23$  (4.3063, 1.9216, 0.4517); and (d)  $\mu=4.30$  (4.5701, 1.6765, 0.4573). The power spectra are based on 2048-point FFT's. In (a) 3000  $x$ - $y$  points are plotted; (b) 3000 points; (c) 6000 points; and (d) 12 000 points.

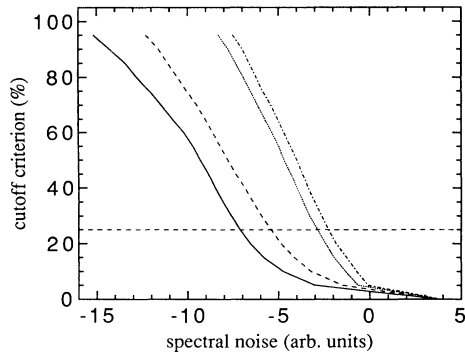


FIG. 6. The relation between cutoff criterion and spectral noise. The criterion gives the percentage of the spectral components that have power less than a given power  $p$ . The figure demonstrates the robustness of the spectral noise measurement to the choice of cutoff criterion, using power spectra from the Rössler system. See Fig. 5 and its caption for details on the Rössler states used. The solid curve corresponds to Rössler system (a); the dashed curve corresponds to Rössler system (b); the dotted curve corresponds to Rössler system (c); and the dot-dash curve corresponds to Rössler system (d). The horizontal dashed line is the 25% criterion.

6 is that the relative spectral noise of the four Rössler states does not change as the cutoff percentage is increased. We obtained similar results from calculating the spectral noise for the combined sine waves with and without the addition of random noise; the spectral noise measurement was robust in this system too. The robustness of the spectral noise gave us confidence that the 25% criterion would yield important information about bifurcations among ordered and disordered states in nonaxisymmetric TC flow.

We also used the Rössler system to characterize further the SMN, but we found that in this case the SMN did not yield conclusive results: There was no significant change in  $D$  as the system became more complex. This finding was consistent with that of Crutchfield *et al.* [30]. We suspect that the SMN was inconclusive for the Rössler system because even in its most chaotic state, the power spectra were composed of dominant, though broad, peaks. For example, the spectra of Figs. 5(a), 5(b), 5(c), and 5(d) had  $D = 2.28, 2.46, 2.34,$  and  $2.35,$  respectively. Measurements of the relative noise from the SND yielded results that were more convincing that those from the SMN. Using the 25% criterion, we found that the spectral noise increased steadily as the Rössler system became more complex; for the spectrum of state  $a$  the spectral noise was  $-12.08,$  for  $b$  the spectral noise was  $-10.04,$  for  $c$  the spectral noise was  $-6.54,$  and for  $d$  the spectral noise was  $-5.86.$

### B. Constructing the bifurcation map

Our use of the SND and SMN allowed us to complete the bifurcation map for the nonaxisymmetric TC system. To determine where a bifurcation occurred in  $\Omega$ - $\Delta$  space, we plotted each of the four statistics as a function of the parameter being varied. We then looked for a sharp, sys-

tematic change in the behavior of that statistic. A bifurcation was determined to have occurred when the statistic changed locally by  $\sim 50\%$ . Figure 2 shows points where the relative reflectance had dropped by 50% (or risen, depending on the direction from which the bifurcation boundary was approached), thus indicating the primary bifurcation. Also presented are the theoretical predictions for the primary bifurcation [10,23]. For the primary bifurcation, our method of detecting bifurcations yielded results that were in good agreement with theory, small  $\Omega$ . The measurements used in Fig. 2 also agreed well with previous measurements using a slightly different method [6].

We applied the 50%-change method to our data, and the resulting bifurcation map is shown in Fig. 7. The symbols are the experimental points. For clarity we have not displayed all of the experimental points. The curves are best fits to the experimental data (including those points not displayed) using a nonlinear least-squares fit to functions of the form

$$\Delta(\Omega) = a\Omega^6 + b\Omega^4 + c\Omega^2 + d. \quad (4)$$

The fits are provided as visual guides through the data. Odd-order terms are not included in the fit because theory predicts [8,10,11], and experiments confirm [6] that the Coriolis force interacts symmetrically with the flow in the sense that  $\pm\Omega$  produces the same changes in bifurcation behavior. The squares and the solid curve represent the bifurcation boundary separating the base flow state from the secondary flow states. The experimental points correspond to those shown in Fig. 2; this is the boundary at which the relative reflectance has changed sharply. Similarly, the circles and the dashed curve indicate the boundary separating the time-independent flow state within the secondary flow (i.e.,

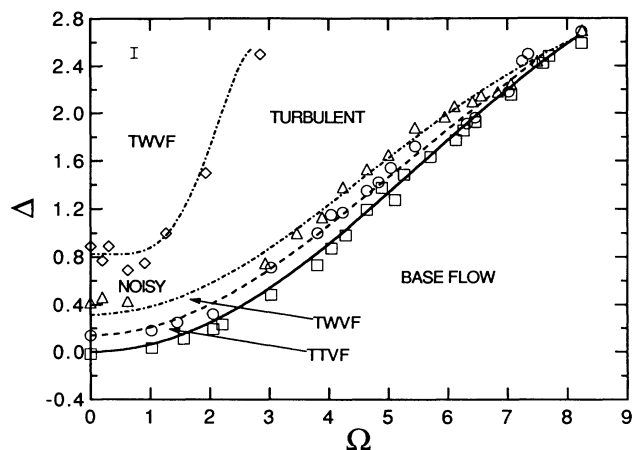


FIG. 7. The bifurcation map for nonaxisymmetric Taylor-Couette flow ( $\eta = 0.880$ ). See the text for a description. Note that for clarity the fit to the variance data (circles) was not shown for data above  $\Omega = 7.5$ . Note also that at  $\Omega = 0$  there is no Coriolis force and so the Taylor vortices and wavy vortices are no longer tilted; the  $\Omega = 0$  boundary is consistent with that for ordinary TC flow. The error bar is an estimate of the error in determining the bifurcation point.

TTVF) from the time-dependent flow states. This boundary is where the variance of the reflectance has changed relatively sharply. The triangles and the dash-dot curve separate TWVF (periodic, ordered flow) from disordered flow (either noisy or turbulent). This boundary was determined by detecting sharp changes in the spectral noise (using the SND). Finally, the diamonds and their accompanying dash-dot curve are the other boundary separating ordered from disordered flow; this boundary was also found using the SND to estimate the spectral noise. As explained earlier, the SMN and the SND provide similar information about a system. We chose to use the SND for the bifurcation map because in practice it was slightly easier to determine bifurcations from the spectral noise than from the SMN. The error bar in the upper left corner of Fig. 7 is an estimate of the error in determining the point at which the bifurcations occur. This uncertainty is primarily due to the uncertainty in choosing where sharp breaks occur in the data.

## V. DISCUSSION

The bifurcation map shows the five states that have been distinguished by their differences in terms of the statistics we employed in our analysis (see Sec. IV). The base flow state is time independent and essentially laminar (although as  $\Omega$  gets large, some structure is observed, appearing as two long curving axial streaks of Kalliroscope; we speculate that the platelets are caught in two stagnation zones that are created from the turnaround regions of the axial flow). The base state is thus characterized by high relative reflectance, low variance, low spectral noise, and low SMN.

TTVF is a time-independent, axially periodic flow. It is characterized by low relative reflectance (since the base state has bifurcated) and lower variance. The spectral noise and SMN are also lower than they were in the base state. The drop in the variance and the noise in the power spectra occur because in TTVF the platelets are less likely to wobble randomly in this more structured state.

TWVF is an ordered, spatiotemporally periodic state identified by low reflectance, a sharp rise in the variance, and a slight increase in both the spectral noise and the SMN.

We have identified two disordered states within the time-dependent flow regime: noisy flow and turbulent flow. These two disordered states are distinguished from TWVF by their large increase in spectral noise and SMN. The difference between noisy flow and turbulence is that noisy flow has strong spatiotemporal periodicity accompanied by an elevation in the power spectral noise. This increase in disorder is not apparent in the flow visually, however. Turbulent flow is highly mixed and disordered, both visually and spectrally.

We observed that, as  $\Delta$  is increased at constant  $\Omega$ , the turbulence grows in as a strong swirling pumping action from the ends and, when fully developed, displays no temporal periodicity and only ghosts of the tilted vortices. One might suspect that the turbulence is driven by end effects. However, Ning *et al.* observed a similar bi-

furcation to turbulence in nonaxisymmetric TC flow using an apparatus with "soft" boundary conditions that do not constrain the tilted vortices at the ends [15]. Their results thus suggest that the turbulent flow we have observed is not an end effect.

Although we have made a distinction between noisy and turbulent flow, we have not been able to define a sharp boundary separating them. Our measurements indicate that the noisy flow continuously becomes more spatiotemporally disordered as the system approaches turbulence. This would be similar to the gradual transition to turbulence from chaos in ordinary TC flow [9,19,20].

Several interesting bifurcation sequences in the nonaxisymmetric TC system are revealed by the bifurcation map. The map shows that the bifurcation behavior of ordinary TC flow is markedly different from that observed in the ordinary system. Specifically, we observe two nonhysteretic bifurcation sequences that display reemergent order. In addition, above a sufficient value of  $\Omega$ , the flow bifurcates nonhysteretically to turbulence directly from the time-independent base state. It should be noted that reemergent order and turbulence both occur in ordinary TC flow, but at Reynolds numbers at least an order of magnitude *higher* than those observed in the nonaxisymmetrically perturbed system.

### A. Reemergent order

Reemergent order is characterized in parameter space by a disordered state bracketed by ordered states. In ordinary TC flow there are known instances of reemergent order, but they are either hysteretic or they occur at Reynolds numbers much larger than those used in the experiments we are reporting.

Hysteretic reemergent order occurs at  $\Omega=0$  in the approximate range  $0.35 < \Delta < 0.8$ , and this is shown on our bifurcation map. Donnelly *et al.* [17] and King and Swinney [16] reported that the region of disorder they observed resulted from eigenstate instabilities in WVF, whereby the number of waves and/or vortices changed. In this unstable WVF state the flow appeared disordered, both visually and spectrally. Visually, a dislocation in the vortex array was observed. The power spectra were characterized by a broadening of the peaks and an increase in the noise significantly above the instrumental level. In addition, the bifurcations through this disordered state were hysteretic. In other words, as the Reynolds number was increased, the system reorganized itself (by changing states), but the initial state could not be recovered by decreasing the Reynolds number back through the bifurcation boundary. We repeated the measurements of Donnelly *et al.* [17] and confirmed their findings by detecting a rise in both the SMN and the spectral noise as the system passed through this disordered state. This hysteretic bifurcation sequence can be seen in Fig. 8, which is a plot of the spectral noise for  $\Omega=0$ . The solid curve is for  $\Delta$  increasing and the dashed curve is for  $\Delta$  decreasing. At  $\Delta=0$ , the bifurcation to TVF can be seen by the drop in the spectral noise. At  $\Delta \approx 0.14$ , the spectral noise rises, indicating the bifurcation to WVF. These changes in the spectral noise are rel-

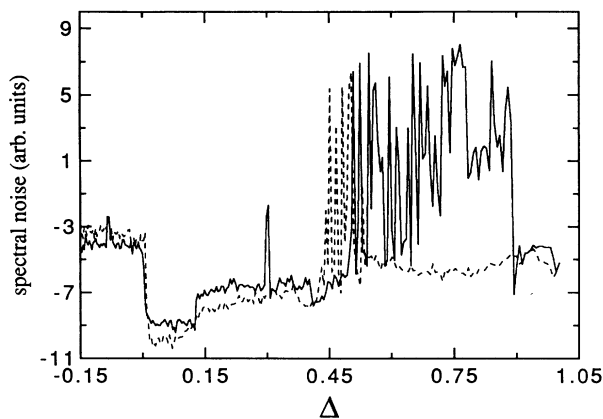


FIG. 8. Spectral noise vs  $\Delta$  at  $\Omega=0$ , showing hysteretic reemergent order. The solid curve represents  $\Delta$  increasing and the dashed curve is for  $\Delta$  decreasing.

atively slight, however, when compared to that for the bifurcation to noisy flow that occurs at  $\Delta \cong 0.50$ . This noisy state persists until  $\Delta \cong 0.90$ , at which point the spectral noise drops back down and remains relatively low. When  $\Delta$  is brought back toward its initial value, we see that the bifurcation sequence for  $\Delta$  increasing does not repeat itself. For  $\Delta$  decreasing, we do see a narrow band of disorder between  $\Delta \cong 0.5$  and  $0.45$ , but it is clear that the bifurcation sequence displaying reemergent order is hysteretic for  $\Omega=0$ .

Our experiments have shown that for  $\Omega \neq 0$  the situation is quite different. As  $\Delta$  is increased, the flow still passes through a region of disorder, but within the approximate range  $0.6 \leq \Omega \leq 2.5$ , the bifurcations no longer display hysteresis. This sequence of bifurcations, from TWVF to disordered flow back to TWVF, can be seen clearly in Figs. 9 and 10, which are typical of the bifurcations between  $0.6 \leq \Omega \leq 2.5$ . Figure 9 shows the spectral noise, measured using the 25% criterion from the SND, as a function of  $\Delta$  for  $\Omega=0.62$ . As  $\Delta$  is increased (solid curve), the spectral noise is relatively low. At about

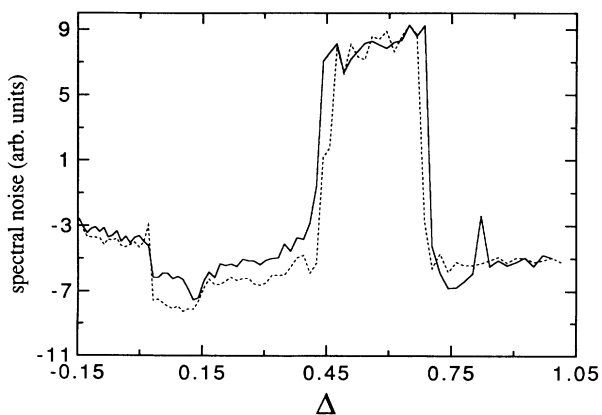


FIG. 9. Spectral noise vs  $\Delta$  at  $\Omega=0.62$ , showing nonhysteretic reemergent order. The solid curve represents  $\Delta$  increasing and the broken curve is for  $\Delta$  decreasing.

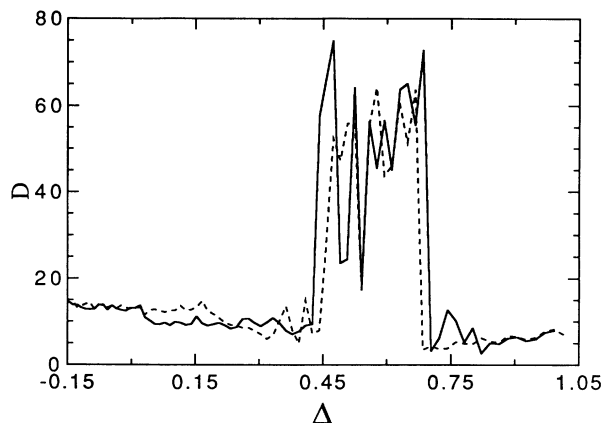


FIG. 10. Spectral mode number  $D$  (where  $D$  is dimensionless) vs  $\Delta$  at  $\Omega=0.62$ , showing nonhysteretic reemergent order. The solid curve represents  $\Delta$  increasing and the dashed curve is for  $\Delta$  decreasing.

$\Delta=0.45$ , there is a sharp increase in the spectral noise; for  $0.45 \leq \Delta \leq 0.68$ , the flow is disordered. Above  $\Delta=0.68$ , and for the rest of the range in  $\Delta$  explored, the system has bifurcated back to TWVF. After the ordered state reemerged in the flow, we quasistatically decrease  $\Delta$ . The dashed curve in Fig. 9 is a plot of the spectral noise versus  $\Delta$  for decreasing  $\Delta$ . It is clear that the bifurcation sequence nearly replicates itself; from this we conclude that for a sufficient value of  $\Omega$ , the flow experiences nonhysteretic reemergent order. Figure 10 shows the SMN versus  $\Delta$  at  $\Omega=0.62$  for this same sequence of bifurcations. Figure 10 confirms that the flow undergoes a series of bifurcations that display nonhysteretic reemergent order. Figures 9 and 10 also indicate that the SND and the SMN do provide consistent information about the bifurcation behavior of our system. Finally, note that the measurements yielding Figs. 8, 9, and 10 were made at the same  $a^*$  ( $a^*=0.66$ ). Thus the bifurcation sequence shown in Fig. 8 can be considered dynamically distinct from that shown in Figs. 9 and 10.

We looked at the nonhysteretic reemergent order in another way by examining the general characteristics of the power spectra for ordered flow (TWVF) versus those of the disordered state. We then compared the profiles of the SND for these states. Figure 11 shows the power spectra for TWVF [Fig. 11(a)], noisy flow [Fig. 11(b)], and the reemerged TWVF [Fig. 11(c)]. These three spectra are accompanied by their respective SND's [Figs. 11(d)–(f)]. The power spectra were constructed by calculating the FFT's from 8192-point reflectance time series. The spectra shown in Fig. 11 have 2048 bins. The data represented in Fig. 11 were acquired at  $\Omega=0.62$ , the same  $\Omega$  at which the measurements of Figs. 9 and 10 were made. The significant increase in the broadband spectral noise in Fig. 11(b) as compared to Fig. 11(a) is indicative of a bifurcation to noisy flow. The SND's for Figs. 11(a)–11(c) show how the power in the spectra is redistributed as the flow goes through a disordered regime. The spectral noise, determined using the 25% criterion, is indicated by the vertical dashed lines in Figs. 11(d)–11(f).

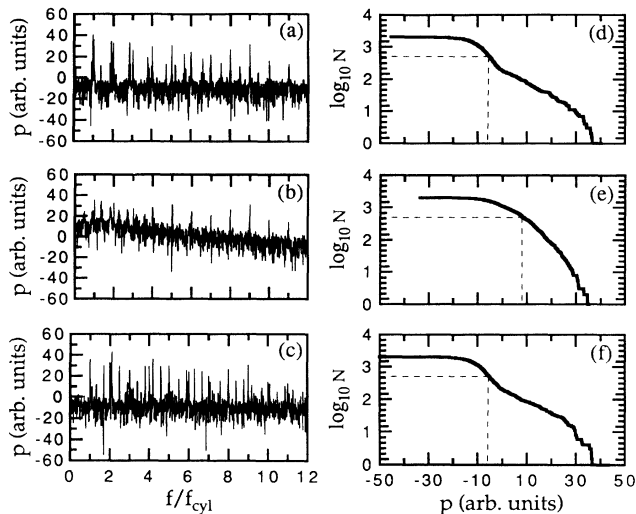


FIG. 11. Power spectra and spectral number distributions of representative data showing reemergent order. (a), (b), and (c) are the power spectra; (d), (e), and (f) are their corresponding SND's. The system is ordered in the states shown in (a) and (c), and (d) and (f). (b) and (e) show the spectral features of noisy flow. The measurements were made at  $\Omega=0.62$ .  $\Delta=0.24$  for (a) and (d),  $\Delta=0.59$  for (b) and (e), and  $\Delta=1.01$  for (c) and (f). In (d)–(f) the horizontal dashed lines indicates  $N = \log_{10}(0.25n)$ , and the vertical dashed lines indicate the spectral noise measured using the 25% criterion.

Note that in Fig. 11(b) there remain sharp spectral peaks even though the noise level has risen significantly. As stated earlier, what we have identified as noisy flow is characterized by an increase in broadband noise above the instrumental level, accompanied by spectral components that indicate that the flow is still strongly periodic. Two other aspects of Fig. 11(b) are important. The first is that this power spectrum is reminiscent of the spectra observed by Brandstater and Swinney for chaotic ordinary TC flow [20]. The second important aspect of Fig. 11(b) is its marked difference from a typical spectrum measured for turbulent flow in our system. Figure 12

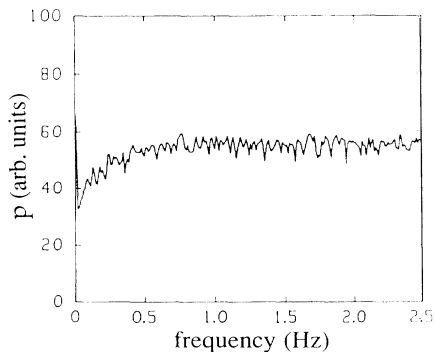


FIG. 12. Typical power spectrum for turbulent flow. Here,  $\Omega=10.41$  and  $\Delta=3.78$ . This figure was generated using a commercial spectrum analyzer with 256-channel resolution.

shows spectral behavior for flow in the turbulent regime. This figure, although plotted on a different scale, does not have any sharp components and the noise level is quite high. Visual observations of the flow confirm that the state represented by Fig. 12 is turbulent: No wavy motion is detectable, there is a high degree of irregularity and mixing in the flow, and there are disordered structures down to the smallest visible length scale. In contrast, the disorder in the noisy state is not apparent visually even though it is quite striking spectrally.

The bifurcation map also indicates that the flow undergoes reemergent order as  $\Omega$  is increased at constant  $\Delta$ . For  $\Omega=0$ , and above  $\Delta=0.14$ , the flow is time dependent, that is, the relative reflectance is low and the variant of the reflectance is relatively high. We have shown that there is a region of disordered flow between  $\Delta \cong 0.35$  and  $0.8$  (see Fig. 8). Above  $\Delta \cong 0.8$ , the disordered flow returns to periodic flow. If we now turn on the Coriolis force and increase  $\Omega$ , a boundary is encountered across which there is a sharp rise in the spectral noise, while the reflectance remains low and the variance high. This indicates that the flow has become disordered; only here it is turbulent as opposed to the noisy state found at lower  $\Omega$ . Also, there was hysteresis in this bifurcation to turbulence, although it was very small compared to the hysteresis shown in Fig. 8. As  $\Omega$  is increased further, the spectral noise drops and TWVF reemerges (the reflectance remains low and the variance remains high). At slightly higher  $\Omega$ , the variance drops indicating that the flow has bifurcated to TTVF. Finally, the flow bifurcates to its base state as signaled by a sharp increase in the relative reflectance. These last three bifurcations were all nonhysteretic.

We have seen that nonaxisymmetric TC flow undergoes reemergent order as a function of either control parameter. That this system displays a broad region of disordered bracketed by ordered states suggests that there are competitive processes occurring in the flow. The two control parameters  $\Omega$  and  $\Delta$  tend to induce flows that, to first order, are orthogonal. Increasing  $\Delta$  at fixed  $\Omega$  means increasing the amount of azimuthal energy in the flow field, hence bringing the system closer to its ordinary state. This tendency back to the ordinary system as  $\Delta$  is increased is particularly important at low  $\Omega$  where the symmetry-breaking perturbation can still be considered small. Furthermore, for low  $\Omega$  we find that as  $\Delta$  is increased, the tilt angle of the vortices is decreased. Conversely, increasing  $\Omega$  for fixed  $\Delta$  induces a stronger axial flow and forces the system farther from ordinary TC flow. Recall from Sec. II B that to first order the axial flow is an  $m=1$  mode, varying sinusoidally about the azimuth. This mode is orthogonal to WVF, and induces the tilt in the wavy vortices.

In the region in  $\Omega$ - $\Delta$  space where neither parameter can establish dominating modes, the flow exhibits an increase in the power spectral noise which we attribute to mode competition. This rise in the spectral noise, and its nonwhite distribution suggest that the noise is deterministic. Since the flow is not strongly turbulent and since this increase in noise occurs at low values of the control parameters, this deterministic noise state could be

chaotic.

The role of mode competition in the onset of noisy or chaotic flow is a topic of much current research. For example, Coughlin *et al.* have performed a Navier-Stokes simulation, and a corresponding experiment (using Kalloscope reflectance as their data), in which the calculations and the experimental data revealed an aperiodic flow state resulting from mode competition among the Zhang-Swinney (ZS) and Gorman-Swinney (GS) modulated wavy vortex modes [34]. Our experiments have all occurred at relatively low Reynolds numbers—typically,  $Re < 3Re_{c0}$ . With the appropriate addition of a small Coriolis force to the Navier-Stokes equations, theoretical progress might be made toward understanding reemergent order in the nonaxisymmetric TC system via numerical simulation or a weakly nonlinear theory. This work might also significantly add to our understanding of the role of mode competition in low-dimensional deterministic noisy flows.

### B. Direct bifurcation to turbulence

The effect of the Coriolis force on the ordinary TC system is seen most profoundly in the direct bifurcation to turbulence. In this phenomenon the flow nonhysteretically bifurcates to turbulence directly from the base state. Furthermore, the Reynolds number at which the bifurcation occurs is an order of magnitude lower than that for the ordinary system. Also, there is a similarity between the direct bifurcation to turbulence in nonaxisymmetric TC flow and a similar bifurcation in Rayleigh-Bénard convection subject to a Coriolis force. Niemela and Donnelly studied this bifurcation (known as the Küppers-Lortz instability) in which the purely conductive state in a rotating Rayleigh-Bénard system becomes unstable and bifurcates to a convective state in which the orientation of the convective rolls switches turbulently [5].

The direct bifurcation to turbulence can be seen in the convergence of the three lower bifurcation boundaries in Fig. 7 as  $\Omega$  increases. Specifically, as  $\Omega$  approaches  $\sim 7.5$ , the boundaries for the drop in relative reflectance, the rise in variance, and the rise in spectral noise gradually converge.

The nature of this convergence is more evident if we examine the coincident behavior of the various bifurcations. For instance, Fig. 13(a) shows the relative reflectance plotted with the variance for increasing  $\Delta$  at constant  $\Omega$  in a parameter space region before the direct bifurcation to turbulence; Fig. 13(b) is a similar plot for measurements in a region beyond the direct bifurcation to turbulence. In Fig. 13(a) the bifurcation to TTVF (indicated by the drop in reflectance) occurs at a lower Reynolds number than the bifurcation to TWVF (indicated by the rise of the variance). When we take the ratio of the Reynolds number for the bifurcation to TTVF,  $Re_c$ , versus the Reynolds number for the bifurcation to time-dependent flow,  $Re_t$ , we find that  $Re_t/Re_c > 1$ . Figure 13(b) also shows strikingly different behavior. Here,  $Re_c$  coincides with  $Re_t$ , such that  $Re_t/Re_c \cong 1$ . In addition, the data display much more fluctuation than those in Fig. 13(a). This fluctuation is suggestive of a qualitative change in the flow beyond  $Re_t$ ; indeed, power spectra

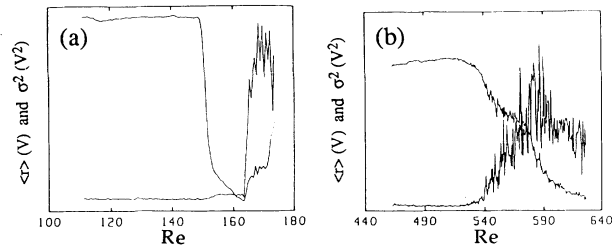


FIG. 13. Average reflectance  $\langle r \rangle$  and variance  $\sigma^2$  plotted simultaneously. The curves that are initially high are the relative reflectance, and the curves that are initially low are the variance of the reflectance. (a)  $\Omega = 2.08$ . Notice that the transitions do not coincide:  $Re_t/Re_c \cong 1.08$ . (b)  $\Omega = 10.41$ . Notice that the transitions now coincide:  $Re_t/Re_c \cong 1.00$ . Also note the differences in the critical Reynolds numbers in (a) and (b), indicating strong stabilization due to the Coriolis force.

typical of the flow beyond  $Re_t$  in Fig. 13(b) indicate that when  $Re_c$  and  $Re_t$  coincide, the flow bifurcates to turbulence as opposed to TWVF (see Fig. 12).

To examine more closely how the bifurcation boundaries converge, we plotted in Fig. 14,  $Re_t/Re_c$  versus  $\Omega$  and  $Re_n/Re_t$  versus  $\Omega$ , where  $Re_n$  is the critical Reynolds number for the bifurcation to disordered flow. The solid diagonal line in Fig. 14 is a linear fit to the experimental data. The dashed horizontal line indicates where the ratio of the critical Reynolds numbers equals unity. From Fig. 14 we can see that both  $Re_t/Re_c$  and  $Re_n/Re_t$  approach unity as  $\Omega$  approaches 7.5. This means that the bifurcation of the base flow directly to a time-dependent state (i.e.,  $Re_t/Re_c = 1$ ) is coincident with the initial time-dependent state being turbulent (i.e.,  $Re_n/Re_t = 1$ ). Recall Fig. 12 which shows the spectral behavior of the flow for  $\Omega > 7.5$  and for  $\Delta$  beyond the boundary  $Re_n/Re_t = 1$ . This figure indicates that beyond the direct bifurcation to time-dependent flow there are no strong periodic components in the flow. In addition, visual observations confirm what we have learned from the information summarized by Figs. 12–14. We thus conclude that the system undergoes a direct bifurcation to turbulence from the base flow state for a sufficient Coriolis force.

Although the flow bifurcates directly to turbulence from the base state, the bifurcation does not occur sharp-

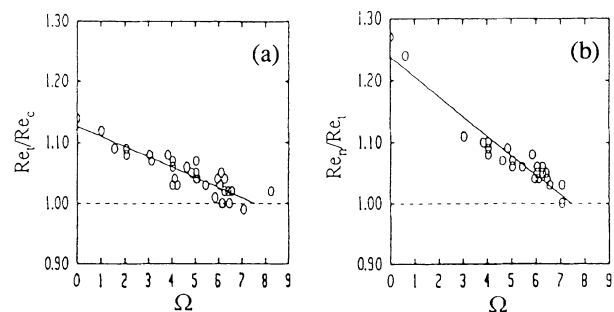


FIG. 14. (a)  $Re_t/Re_c$  vs  $\Omega$ . (b)  $Re_n/Re_t$  vs  $\Omega$ . The solid diagonal line is a linear fit to the experimental data. The dashed horizontal line indicates where the ratio of the critical Reynolds numbers equals unity.

ly [compare Figs. 13(a) and 13(b)]. The turbulence grows in as a function of  $\Delta$ . The region between the initial drop in reflectance and the beginning of the large fluctuations in Fig. 13(b) can best be referred to as a transition region. This transition region was typically about  $\pm 5\%$  of  $\Delta_n$ , where  $\Delta_n$  is the reduced Reynolds number at which the flow bifurcates to disordered flow. Although the turbulence develops in a transition region, the convergence of the bifurcation boundaries implies that the system may display codimension-2 bifurcation behavior.

Codimension-2 bifurcations occur in two-control parameter systems and are of interest because at these points multiple modes are unstable simultaneously [13,34]. As a result, mode competition can occur, giving rise to interesting dynamics and pattern formations, and possibly turbulence. Coughlin *et al.* have theoretical reasons to believe that the direct bifurcation to chaos from a limit cycle (i.e., a periodic state) in ordinary TC flow results from this sort of behavior [34]. They make the conjecture that the aperiodicity they observe results from the mode competition arising from the dynamics around a “bicritical point” separating the ZS and GS modes that occur in MWVF [18,34]. Important insight about a flow can also be had from a weakly nonlinear theory in the vicinity of multicritical or codimension-2 points.

The convergence of the bifurcation boundaries in nonaxisymmetric TC flow strongly suggests that there may be a codimension-2 point in the region  $\Omega \approx 7.5$ ,  $\Delta \approx 2.43$ . Our data indicate that for  $\Omega$  substantially less than 7.5, the flow does not display a direct bifurcation to turbulence for increasing  $\Delta$ ; for  $\Omega$  substantially greater than 7.5, we do observe a direct bifurcation. The fits to the data in Figs. 14(a) and 14(b) indicate that  $\Omega = 7.5$  is the convergence point for the critical points  $Re_c$ ,  $Re_r$ , and  $Re_n$ . However, our experiments lacked the necessary precision to definitively identify  $\Omega = 7.5$  as a codimension-2 point. We do suspect, though, that with better experimental precision a codimension-2 point could be located in this region.

We believe that there is much interesting work to be done with the nonaxisymmetric TC system in the codimension-2 region we have described. The broken symmetry of this system and the dynamics we have observed suggest that further experiments and theoretical investigations would be of great importance to the fluid dynamics and nonlinear dynamics communities.

## VI. CONCLUSION

Our experiments on Taylor-Couette flow subject to a nonaxisymmetric Coriolis force have shown that a symmetry-breaking perturbation has profound effects on ordinary Taylor-Couette flow. The bifurcation sequence that one observes in the ordinary system is altered by the Coriolis force. Specifically, the base state is modified and stabilized, as are Taylor vortex flow and wavy vortex flow, both of which also have a tilt induced by the Coriolis force. We have found two striking nonhysteretic bifurcation sequences in this system. One is reemergent order, in which the flow bifurcates from a periodic state

to an aperiodic state back to a periodic state as a function of either control parameter. The other sequence is the direct bifurcation to turbulence, whereby the flow bifurcates to a state of a high spatiotemporal disorder directly from the time-independent base state. The value of the  $\Omega$ - $\Delta$  point at which the direct bifurcation occurs appears to be a codimension-2 bifurcation point at which three bifurcation boundaries converge.

We believe there are still several interesting unanswered questions about this system. For instance, do the dynamics in the noisy state display low-dimensional chaos? One way to resolve this question adequately would be to make point velocity measurements with a laser Doppler velocimeter; however, this is an exceedingly difficult task to undertake on a rotating turntable. What happens to the flow at much higher  $\Delta$ , that is, how is quasiperiodic flow affected when the rotational symmetry of the system is broken? It has been suggested that the incommensurate modes might lock if the symmetry of the flow is broken [35]. What sort of theoretical progress might be made on this system, especially in the disordered regimes and around the codimension-2 point? What are the implications to bifurcation theory for systems that have broken symmetry from the outset? And, finally, are there any bifurcation phenomena that occur for Coriolis forces larger than those explored in the work reported here? In particular, are there any time-dependent states that are Coriolis-force induced? For large  $\Omega$ , the flow approaches the geostrophic limit, in which interesting phenomena with geophysical implications are known to occur [7].

## ACKNOWLEDGMENTS

We wish to thank Dr. Sarah A. Little and Mr. Gregory H. Bauer for their assistance with data analysis. Professor Guenter Ahlers, Professor Greg King, Dr. Ning Li, Professor Kwangjai Park, Dr. Charles Swanson, Professor Randall Tagg, and Professor Morten Tveitereid contributed valuable suggestions and insights. We also wish to acknowledge the talents and input of the late Don Nickles who built and modified the apparatus used in the experiments reported here. This research has been supported by the NSF Low Temperature Physical Program under Grant No. DMR-8815803. Support was also provided to P.W.H. by the Office of Naval Technology.

## APPENDIX

To break the axisymmetry of the ordinary TC system, the Taylor-Couette cylinders must be placed such that their common rotation axis is nonparallel to the rotation axis of the turntable. We will show below that if the axes are parallel, the only effect will be to vectorially add the turntable rotation to that of the cylinders. Furthermore, the location of the cylinders relative to the center of the table does not affect the fluid dynamics. This is because any radial dependence enters the equations of motion through the centrifugal force, and as we will also show, the centrifugal force simply adds to the pressure gradient term, yielding an effective pressure. In the absence of

TABLE I. Theoretical predictions and experimental measurements of  $Re_{c1}$  and  $Re_{c2}$ .

$\Omega_D$	$Re_{c2}$		Diff. (%)	$Re_{c1}$		Diff. (%)
	Theor.	Expt.		Theor.	Expt.	
0.10	14.74	14.74	0	122.44	122.06	0.31
		14.74	0		121.93	0.42
0.20	29.43	29.48	-0.17	126.35	125.83	0.41
0.30	44.67	44.22	1.01	132.38	131.01	1.03

density gradients (that is, if the fluid is homogeneous), the pressure gradient is a static force similar to the gravitational force, and hence does not affect the flow dynamically.

The Navier-Stokes equations for a flow in a rotating reference frame are

$$\frac{\partial \mathbf{u}}{\partial t} = \nu \nabla^2 \mathbf{u} - (\mathbf{u} \cdot \nabla) \mathbf{u} - \frac{1}{\rho} \nabla p' - \Omega_D \times (\Omega_D \times \mathbf{r}) - 2\Omega_D \times \mathbf{u}, \quad (\text{A1})$$

where  $\mathbf{u}$  is the three-dimensional velocity field,  $\rho$  is the density of the fluid,  $p'$  is the pressure, and  $\Omega_D$  is the rotational vector of the reference frame [7]. The continuity equation is

$$\nabla \cdot \mathbf{u} = 0. \quad (\text{A2})$$

The double cross product in Eq. (A1) is the centrifugal force term, and it can be rewritten as the gradient of a scalar:

$$\Omega_D \times (\Omega_D \times \mathbf{r}) = -\nabla \left( \frac{1}{2} \Omega_D^2 r'^2 \right), \quad (\text{A3})$$

where  $r'$  is the distance from the axis of rotation. If the fluid is homogeneous, then the pressure in Eq. (A1) can be combined with the right-hand side of Eq. (A3) and expressed as an effective pressure  $p$ :

$$p = p' - \frac{1}{2} \rho \Omega_D^2 r'^2. \quad (\text{A4})$$

Combining Eq. (A4) with Eq. (A1) yields the appropriate equation of motion for our system,

$$\frac{\partial \mathbf{u}}{\partial t} = \nu \nabla^2 \mathbf{u} - (\mathbf{u} \cdot \nabla) \mathbf{u} - \frac{1}{\rho} \nabla p - 2\Omega_D \times \mathbf{u}. \quad (\text{A5})$$

The pressure gradient is simply modified by the centrifugal force, and the modified pressure does not affect the dynamics since the fluid is assumed to be homogeneous. Ning, Ahlers, and Cannell experimentally verified that centrifugal effects could indeed be ignored in the nonaxisymmetric TC system by placing their apparatus in various radial positions on a turntable [14]. They did not notice any dependence of the flow on the radial position of the cylinders. We obtained similar results in our laboratory.

We can now examine the effect of placing the cylinders' rotation axis parallel to that of the turntable. Let  $\omega_1$  be the inner-cylinder rotation vector,  $\omega_2$  the outer-cylinder rotation vector, and  $\mu = (\omega_2/\omega_1)$  their ratio. The solution of the Navier-Stokes equations for ordinary TC flow is

$$v = Ar + \frac{B}{r}, \quad (\text{A6})$$

where  $v$  is the component of  $\mathbf{u}$ :  $\mathbf{u}(r, \theta, z) = (u, v, w)$  [7]. In Eq. (A6),  $r$  is the distance from the cylinder axis.  $A$  and  $B$  are constants that depend on  $\omega_1$ , the radius ratio  $\eta$ , and  $\mu$ . The pressure field in the azimuthal base state of ordinary TC flow is

$$p = \rho \int \frac{v^2}{r} dr. \quad (\text{A7})$$

If  $\omega_1$  and  $\omega_2$  are parallel to  $\Omega_D$  and if we apply the assumptions that enter into the derivations of Eqs. (A6) and (A7) [7], then we get Eq. (A6) as a solution to the Navier-Stokes equations. The difference is that  $\omega_1 \rightarrow \omega_1 + \Omega_D$ , and  $\omega_2 \rightarrow \omega_2 + \Omega_D$ , so that  $\mu$ ,  $A$ , and  $B$  are changed appropriately. We do find, however, that the pressure is modified:

$$p = \rho \int \left[ \frac{v^2}{r} + \Omega_D v \right] dr. \quad (\text{A8})$$

Again, this modification to the pressure will not have any effect on the fluid dynamics as long as the fluid is homogeneous.

We theoretically and experimentally verified that in the parallel orientation,  $\Omega_D$  would simply add to the cylinder rotation vectors and result in bifurcations to Taylor vortex flow consistent with the results for corotating or counterrotating cylinders. Our predictions were formulated using the technique described by Wiener, Hammer, and Tagg for  $\mu \neq 0$  [10]. With  $\omega_2 = 0$ , we get  $\mu = \Omega_D / (\omega_1 + \Omega_D)$ , and our calculations resulted in predicted values for  $Re_{c1}$  and  $Re_{c2}$  (which are the inner- and outer-cylinder critical Reynolds numbers, respectively) for various values of  $\Omega_D$ . We then performed experiments to measure the primary bifurcation at these values of  $\Omega_D$ . Our theoretical predictions and experimental measurements of  $Re_{c1}$  and  $Re_{c2}$  are shown in Table I. Within the range investigated, our theory and experimental measurements agreed to within 1%.

We have demonstrated two important conclusions about our system. The first is that centrifugal effects can be safely ignored, at least at the small rotation rates we used. The second is that parallel orientation is equivalent to corotation (or counter-rotation in the case of antiparallel orientation) of the concentric cylinders. To break the axisymmetry of the ordinary TC system, the cylinders must be placed so that their rotation axes are nonparallel to the rotation axis of the turntable.

\*Present address: Code R44, NavSWC, Silver Spring, MD 20903-5000;

electronic address: bo@critical.nswc.navy.mil

†Present address: College of Oceanography, Oregon State University, Corvallis, OR 97331-5503; electronic address: rwiener@oce.orst.edu

- [1] S. Chandrasekhar, *Hydrodynamic and Hydromagnetic Stability* (Clarendon, Oxford, 1961).
- [2] Y. Nakagawa, *Nature* **175**, 417 (1955).
- [3] R. J. Donnelly and M. Ozima, *Proc. R. Soc. London, Ser. A* **266**, 273 (1962).
- [4] D. Fultz, Y. Nakagawa, and P. Frenzen, *Phys. Rev.* **94**, 1471 (1954).
- [5] J. J. Niemela and R. J. Donnelly, *Phys. Rev. Lett.* **57**, 2524 (1986).
- [6] R. J. Wiener, P. W. Hammer, C. E. Swanson, and R. J. Donnelly, *Phys. Rev. Lett.* **64**, 1115 (1990).
- [7] D. J. Tritton, *Physical Fluid Dynamics* (Clarendon, Oxford, 1988).
- [8] R. J. Wiener, P. W. Hammer, C. E. Swanson, D. C. Samuels, and R. J. Donnelly, *J. Stat. Phys.* **64**, 913 (1991).
- [9] R. C. Di Prima and H. L. Swinney, in *Hydrodynamic Instabilities and the Transition to Turbulence*, 2nd ed., edited by H. L. Swinney and J. P. Gollub (Springer-Verlag, Berlin, 1985).
- [10] R. J. Wiener, P. W. Hammer, and R. P. Tagg, *Phys. Rev. A* **44**, 3653 (1991).
- [11] L. Ning, M. Tveitereid, G. Ahlers, and D. S. Cannell, *Phys. Rev. A* **44**, 2505 (1991).
- [12] W. F. Langford, R. Tagg, E. J. Kostelich, H. L. Swinney, and M. Golubitsky, *Phys. Fluids* **31**, 776 (1988).
- [13] M. Golubitsky, I. Stewart, and D. Shaeffer, *Singularities and Groups in Bifurcation Theory* (Springer-Verlag, New York, 1988), Vol. II.
- [14] L. Ning, G. Ahlers, and D. L. Cannell, *J. Stat. Phys.* **64**, 927 (1991).
- [15] L. Ning, G. Ahlers, D. S. Cannell, and M. Tveitereid, *Phys. Rev. Lett.* **66**, 1575 (1991).
- [16] G. P. King and H. L. Swinney, *Phys. Rev. A* **27**, 1240 (1983).
- [17] R. J. Donnelly, K. Park, R. Shaw, and R. W. Walden, *Phys. Rev. Lett.* **44**, 987 (1980).
- [18] M. Gorman and H. L. Swinney, *Phys. Rev. Lett.* **43**, 1871 (1979); L. Zhang and H. L. Swinney, *Phys. Rev. A* **31**, 1006 (1985).
- [19] J. P. Gollub and H. L. Swinney, *Phys. Rev. Lett.* **35**, 927 (1975).
- [20] A. Brandstater and H. L. Swinney, *Phys. Rev. A* **35**, 2207 (1987).
- [21] R. W. Walden and R. J. Donnelly, *Phys. Rev. Lett.* **42**, 301 (1979).
- [22] I. Mutabazi, J. J. Hegseth, and C. D. Andereck, *Phys. Rev. A* **38**, 4752 (1988); I. Mutabazi, J. J. Hegseth, C. D. Andereck, and J. E. Wesfreid, *Phys. Rev. Lett.* **64**, 1729 (1990); I. Mutabazi and C. D. Andereck, *Phys. Rev. A* **44**, R6169 (1991).
- [23] M. Tveitereid, L. Ning, and G. Ahlers (private communication and unpublished).
- [24] P. Matisse and M. Gorman, *Phys. Fluids* **27**, 759 (1984).
- [25] P. W. Hammer, Ph.D. dissertation, University of Oregon, 1991.
- [26] K. Park, G. L. Crawford, and R. J. Donnelly, *Phys. Rev. Lett.* **47**, 1448 (1981).
- [27] K. Park and K. Jeong, *Phys. Rev. A* **31**, 3457 (1985).
- [28] Ö. Savas, *J. Fluid Mech.* **152**, 235 (1985).
- [29] K. Schwarz, *Phys. Rev. Lett.* **64**, 415 (1990).
- [30] J. Crutchfield, D. Farmer, N. Packard, R. Shaw, G. Jones, and R. J. Donnelly, *Phys. Lett. A* **76**, 1 (1980).
- [31] K. Park and R. J. Donnelly, *Phys. Rev. A* **24**, 2277 (1981).
- [32] K. L. Babcock, G. Ahlers, and D. S. Cannell, *Phys. Rev. Lett.* **67**, 3388 (1991).
- [33] W. L. Ditto, M. L. Spano, H. T. Savage, S. N. Rauseo, J. Heagy, and E. Ott, *Phys. Rev. Lett.* **65**, 533 (1990).
- [34] K. T. Coughlin, P. S. Marcus, R. P. Tagg, and H. L. Swinney, *Phys. Rev. Lett.* **66**, 1161 (1991).
- [35] P. S. Marcus (private communication).

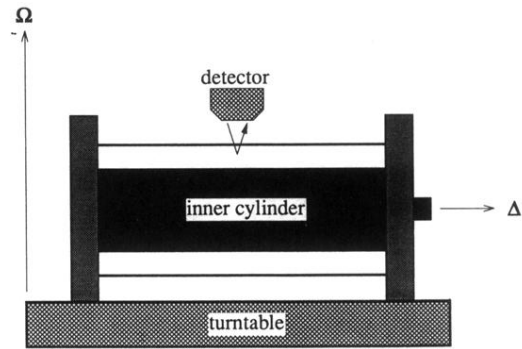


FIG. 1. Side-view schematic of the experimental configuration, showing the orientation of the cylinders relative to the turntable and the orientation of the reflectance detector.